university of groningen

University Medical Center Groningen

University of Groningen

Crystallographic studies of the interactions of Escherichia coli lytic transglycosylase Slt35 with peptidoglycan

Asselt, Erik J. van; Kalk, Kor H.; Dijkstra, Bauke W.

Published in:
Biochemistry

DOI:
10.1021/bi992161p

IMPORTANT NOTE: You are advised to consult the publisher's version (publisher's PDF) if you wish to cite from it. Please check the document version below.

Document Version
Publisher's PDF, also known as Version of record

Publication date:
2000

Link to publication in University of Groningen/UMCG research database

Citation for published version (APA):
Asselt, E. J. V., Kalk, K. H., & Dijkstra, B. W. (2000). Crystallographic studies of the interactions of Escherichia coli lytic transglycosylase Slt35 with peptidoglycan. Biochemistry, 39(8), 1924-1934. DOI: 10.1021/bi992161p

Copyright
Other than for strictly personal use, it is not permitted to download or to forward/distribute the text or part of it without the consent of the author(s) and/or copyright holder(s), unless the work is under an open content license (like Creative Commons).

Take-down policy
If you believe that this document breaches copyright please contact us providing details, and we will remove access to the work immediately and investigate your claim.

Downloaded from the University of Groningen/UMCG research database (Pure): http://www.rug.nl/research/portal. For technical reasons the number of authors shown on this cover page is limited to 10 maximum.

Download date: 10-02-2018

Crystallographic Studies of the Interactions of *Escherichia coli* Lytic Transglycosylase Slt35 with Peptidoglycan[†,‡]

Erik J. van Asselt, Kor H. Kalk, and Bauke W. Dijkstra*

BIOSON Research Institute, Laboratory of Biophysical Chemistry, University of Groningen, Nijenborgh 4, 9747 AG Groningen, The Netherlands

Received September 17, 1999; Revised Manuscript Received December 6, 1999

ABSTRACT: Lytic transglycosylases catalyze the cleavage of the β-1,4-glycosidic bond between *N*-acetylmuramic acid (MurNAc) and *N*-acetylglucosamine (GlcNAc) in peptidoglycan with concomitant formation of a 1,6-anhydro bond in the MurNAc residue. To understand the reaction mechanism of *Escherichia coli* lytic transglycosylase Slt35, three crystal structures have been determined of Slt35 in complex with two different peptidoglycan fragments and with the lytic transglycosylase inhibitor bulgecin A. The complexes define four sugar-binding subsites (−2, −1, +1, and +2) and two peptide-binding sites in a large cleft close to Glu162. The Glu162 side chain is between the −1 and +1 sugar-binding sites, in agreement with a function as catalytic acid/base. The complexes suggest additional contributions to catalysis from Ser216 and Asn339, residues which are conserved among the MltB/Slt35 lytic transglycosylases.

Lytic transglycosylases catalyze the cleavage of the β-1,4-glycosidic bond between *N*-acetylmuramic acid (MurNAc)[1] and *N*-acetylglucosamine (GlcNAc) residues in peptidoglycan with concomitant formation of a 1,6-anhydro bond in the MurNAc residue (anhMurNAc) (*1*). These bacterial enzymes play a role in peptidoglycan metabolism, but their precise functions are not known. Among others, they have been implicated as space makers for the insertion of new peptidoglycan into the cell wall during remodeling and cell growth (*2*) and as cell wall zippers during cell division (*3*). Furthermore, they may function in the recycling of old peptidoglycan material (*4*) or may make pores in the peptidoglycan layer to allow transport of DNA and proteins across the cell wall (*5*). Because peptidoglycan is unique and essential for bacteria, lytic transglycosylases may be effective targets for drug design (*6*).

Structural research on lytic transglycosylases has so far resulted in the X-ray structures of the 70 kDa soluble lytic transglycosylase Slt70 (*7*) and the 36 kDa soluble lytic transglycosylase Slt35 of *Escherichia coli* (*8*, *9*). Slt35 is a fully active, soluble form of the 40 kDa membrane-anchored lytic transglycosylase B (MltB). Limited proteolysis of the peptide bond between residues 39 and 40 results in the release of Slt35 (residues 40−361) (*10*−*12*). The structure of Slt35 shows three domains named the α, β, and core domains. The core domain resembles the fold of goose-type lysozyme and the catalytic domain of Slt70 (*9*). It contains Glu162, which coincides with the catalytic Glu478 of Slt70 and Glu73 of goose-type lysozyme after superposition. Near Glu162, a deep groove is present in the core domain, where a GlcNAc residue was found to occupy carbohydrate-binding subsite −2 (for binding site nomenclature, see ref *13*). Furthermore, the core domain contains an EF-hand calcium-binding site (*9*, *14*), which is about 20 Å from Glu162. Both Slt35 and Slt70 are exo-muramidases that require the peptide side chains in peptidoglycan for activity (*15*, *16*). It is believed that the N-terminal, doughnut-shaped domain of Slt70 and the "exo-loop" of Slt35 (residues 99−108) impose this exo-muramidase activity (*9*).

To further analyze the active site architecture of Slt35 and to understand its peptidoglycan cleavage mechanism, we determined the binding mode of $(GlcNAc)_2$ (chitobiose), the peptidoglycan fragment GlcNAc-MurNAc-L-Ala-D-Glu (murodipeptide), and the glycopeptide bulgecin A in the active site of Slt35 by X-ray crystallography (see Figure 1 for schematic diagrams of these compounds). Bulgecin A is a natural lytic transglycosylase inhibitor containing a 4-O-sulfonated GlcNAc residue and a 4-hydroxy-5-(hydroxymethyl)-L-proline with a linked taurine residue (*6*, *17*, *18*). This study allows us to define four sugar-binding sites and two peptide-binding sites. Furthermore, the complexes suggest contributions to catalysis from Glu162, Ser216, and Asn339, residues which are conserved among the MltB/Slt35 lytic transglycosylases.

MATERIALS AND METHODS

Crystallization. The Slt35 protein was isolated as described previously (*11*). The resulting protein solution consisted of 28 mg/mL Slt35, 1% polyethylene glycol 20000 (PEG20K),

[†] The investigations were supported by the Netherlands Foundation for Chemical Research (SON) with financial aid from the Netherlands Organisation for Scientific Research (NWO).

[‡] The atomic coordinates described in this paper have been deposited with the Protein Data Bank (entries 1D0K, 1D0L, and 1D0M).

* Corresponding author. E-mail: bauke@chem.rug.nl. Fax: +31 50 363 4800. Telephone: +31 50 363 4378.

[1] Abbreviations: GlcNAc, *N*-acetylglucosamine; chitobiose, *N*-(acetylglucosamyl)-*N*-(acetylglucosamine); MurNAc, *N*-acetylmuramic acid; murodipeptide, *N*-(acetylglucosamyl)-*N*-(acetylmuramyl)-L-alanyl-D-glutamic acid; hydroxyproline, 4-hydroxy-5-(hydroxymethyl)-L-proline; MltB, membrane-bound lytic transglycosylase B; Slt35, 36 kDa soluble lytic transglycosylase; Slt70, 70 kDa soluble lytic transglycosylase; PEG20K, polyethylene glycol 20000.

10.1021/bi992161p CCC: $19.00 © 2000 American Chemical Society
Published on Web 02/03/2000

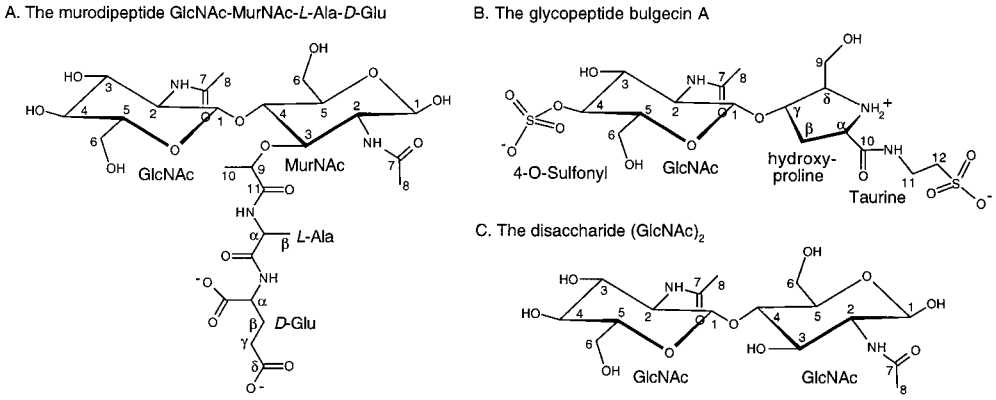

FIGURE 1: Schematic representation of compounds soaked in the Slt35 crystals. (A) The murodipeptide *N*-(acetylglucosamyl)-*N*-(acetylmuramyl)-L-alanyl-D-glutamic acid. (B) The glycopeptide bulgecin A. Bulgecins are produced by *Pseudomonas mesoacidophila* and *Pseudomonas acidophila* in three different forms, A−C (*35*). Bulgecin A constitutes the major component and has linked a taurine residue ($NHCH_2CH_2SO_3$) to the 4-hydroxy-5-(hydroxymethyl)-L-proline (indicated as "hydroxyproline") via an amide bond. Instead of a taurine residue, bulgecins B and C have linked a β-alanine ($NHCH_2CH_2COOH$) or a free OH group. (C) The disaccharide chitobiose, $(GlcNAc)_2$.

150 mM NaCl, and 20 mM HEPES buffer (pH 7.5). Prior to the crystallization experiments, this solution was diluted four times with 10 mM Tris-HCl (pH 7.2) and 1% 2-propanol, and subsequently dialyzed for 6 h against 10 mM Tris-HCl buffer (pH 7.2) and 1% 2-propanol. This was done to remove ethylene glycol, which appeared to be bound in the active site of the native Slt35 structure (*9*) and which probably originated from the PEG20K. The enzyme was crystallized using the hanging drop vapor diffusion method with 3 μL of protein solution and 3 μL of reservoir solution consisting of 0.1 M bicine-NaOH buffer (pH 7.8) only (*8*).

Soaking Experiments. A 25% (w/v) PEG20K stock solution was dialyzed against pure water using a membrane with a 6−10 kDa cutoff for 24 h. The concentration of the PEG20K was determined with a GPR 11-37 refractometer (Index Instruments). The Slt35 crystals were repeatedly washed in a solution of 50 mM Tris-HCl buffer (pH 8.0) and 2% dialyzed PEG20K. Subsequently, one crystal was soaked in a solution of 50 mM Tris-HCl buffer (pH 8.0), 2% dialyzed PEG20K, and 17 mM *N*-(acetylglucosamyl)-*N*-(acetylmuramyl)-L-alanyl-D-glutamic acid (murodipeptide obtained from Sigma) for 4 h. A second crystal was soaked for 18.5 h in a solution of 50 mM Tris-HCl buffer (pH 8.0), 2% dialyzed PEG20K, 1 mM $CaCl_2$, and 20 mM bulgecin A [kindly provided by A. J. Dijkstra (F. Hoffmann-LaRoche Ltd.)]. A third crystal was also soaked in this bulgecin A solution, but after 2 min, it was transferred to a solution of 50 mM Tris-HCl buffer (pH 8.0), 2% dialyzed PEG20K, 1 mM $CaCl_2$, 10 mM bulgecin A, and 10 mM chitobiose (purchased from Sigma) and soaked for $^1/_2$ min.

Data Collection and Processing. For the diffraction experiments, the crystals were flash-frozen at 120 K in a stream of evaporating nitrogen after having been soaked for 30−60 s in a cryoprotectant consisting of 50 μL of 87% glycerol and 50 μL of soaking solution. The Slt35−murodipeptide and Slt35−bulgecin A−chitobiose data were collected in house on DIP image plates (MacScience) using CuKα radiation from a Nonius FR591 rotating anode generator with Franks' mirrors. The Slt35−bulgecin A data set was measured at the X11 beamline of the EMBL outstation at DESY (Hamburg, Germany) using 0.9057 Å radiation and a FastMar-Research image plate detector system. All data were processed with DENZO and SCALEPACK (*19*), and the measured intensities were converted to structure factor amplitudes with programs from the Groningen BIOMOL software package. Data collection statistics can be found in Table 1A.

Refinement. For the refinement, the same reflections that were selected for the R_{free} calculations of the native data set (10% of the reflections) were set aside (*20*). As a starting model, the refined native Slt35 structure to 1.7 Å resolution was used, including the solvent molecules and alternate side chain conformations (*9*). After rigid-body refinement (3.5−8.0 Å resolution), the models were refined in several cycles of Powell energy minimization, occupancy refinement of alternate side chain conformations, and overall and individual *B*-factor refinement with the program X-PLOR, version 3.843 (*21*), and addition of solvent and substrate molecules and manual rebuilding in O (*22*). Only the solvent molecules and alternate side chains with electron density above 1σ in $2F_o - F_c$ maps we kept during the refinement. The force constants and parameters used for the sugars were those described by Weis et al. (*23*) as implemented in the X-PLOR geometry files. The coordinates, parameter file, and topology file of bulgecin A were derived from a desulfonated form of bulgecin (*17*). Low-resolution diffraction data to 20 Å were included, and a bulk solvent correction was applied. The application of an anisotropic *B*-factor scaling and a resolution-dependent and $1/\sigma^2$ weighting scheme resulted in lower R_{free} values and smaller differences between R_{work} and R_{free}. The last refinement cycle was repeated with all data, including the test set. The final refinement statistics for the complex structures are summarized in Table 1B. Stereochemistry was inspected with the program PROCHECK (*24*).

RESULTS

Three crystals of Slt35 were successfully soaked with the murodipeptide *N*-(acetylglucosamyl)-*N*-(acetylmuramyl)-L-alanyl-D-glutamic acid, the glycopeptide bulgecin A, and a mixture of bulgecin A and chitobiose, respectively (Figure 1). In each complex, a calcium ion is bound in the EF-hand calcium-binding site in a fashion similar to that described previously (*14*). The side chain of the first N-terminal residue Met40 and an internal stretch of 8−10 residues (99−108 or 101−108) do not exhibit interpretable electron density in $F_o - F_c$ and $2F_o - F_c$ omit maps and have been omitted

Table 1: Data Collection and Refinement Statistics

	murodipeptide	bulgecin A	bulgecin A and chitobiose
	(A) Data Collection		
resolution (Å) (last shell)	23.2−2.02 (2.05−2.02)	32.8−1.97 (2.00−1.97)	23.6−2.47[e] (2.51−2.47)
no. of total reflections	108180	205843	35069
no. of unique reflection	26200	27987	13028
completeness (%) (last shell)	99.0 (99.9)	99.3 (85.0)	90.3 (69.3)
R_{merge}[a] (%) (last shell)	6.7 (26.7)	5.3 (24.9)	3.7 (11.8)
unit cell dimensions (*a*, *b*, *c* in Å)	58.4, 67.8, 98.9	58.4, 67.8, 97.7	58.6, 67.8, 97.8
	(B) Refinement		
resolution range (Å)	20.0−2.02	20.0−1.97	20.0−2.47
no. of total reflections	25892	27351	12912
no. of reflections in work set	23291	24588	11633
final *R*-factor (%)[b]	16.8	17.0	17.9
R_{work} (%)[b]	16.5	16.8	17.4
R_{free} (%)[b]	20.2	20.0	24.1
rmsd			
bond lengths (Å)[c]	0.006	0.006	0.007
bond angles (deg)[c]	1.2	1.2	1.3
dihedral angles (deg)[c]	21.8	21.7	22.3
improper angles (deg)[c]	1.04	1.05	1.03
no. of non-H protein atoms	2546	2537	2508
no. of residues	40−100, 109−361	40−100, 109−361	40−98, 109−361
no. of alternate side chains	12	10	6
no. of water molecules	362	286	200
no. of substrate atoms	96	35	65
no. of calcium ions	1	1	1
no. of glycerol molecules	1	0	0
average *B*-factor (Å^2)			
all atoms	18.2	23.5	31.7
main chain atoms	14.1	19.9	30.4
side chains	16.9	23.2	31.2
glycerol	23.3	−	−
murodipeptide[d]			
GlcNAc	20.7 (A), 37.9 (B)		
MurNAc	23.1 (A), 51.1 (B)		
L-Ala	23.7 (A), 65.5 (B)		
D-Glu	25.5 (A), 67.2 (B)		
bulgecin A			
4-*O*-sulfonyl-GlcNAc		25.4	28.6
hydroxyproline		20.0	25.3
taurine		50.1	50.8
chitobiose			
GlcNAc +1			42.2
GlcNAc +2			51.0

[a] $R_{merge} = \Sigma|I - \langle I\rangle|/\Sigma I$. [b] *R*-factor $= \Sigma||F_{obs}| - |F_{calc}||/\Sigma|F_{obs}|$. R_{work} and R_{free} are defined for reflections with $F > 0$. The final *R*-factor is calculated for all reflections with $F > 0$ in the resolution range. [c] With respect to the parameters of Engh and Huber (*34*). [d] Muropeptide A is bound in subsites −2 and −1; muropeptide B is found in subsites +1 and +2. [e] The effective resolution is 2.57 Å.

from the models. All residues are found in the allowed regions of the Ramachandran diagram according to PROCHECK (*24*) and have good stereochemistry. Details of the structure determinations of the three complexes are summarized in Table 1.

Slt35−Murodipeptide Complex. Two murodipeptides (murodipeptides A and B) were found to be bound in the active site cleft of Slt35 (Figure 2A). Murodipeptide A binds with its GlcNAc and MurNAc residues in subsites −2 and −1, respectively, while murodipeptide B occupies subsites +1 and +2 (Figures 3A and 4A). Because its electron density was weak, murodipeptide A was refined with an occupancy of 0.5. However, some residual density remained at subsites −2 and −1, in which a glycerol molecule and six water molecules could be placed with an occupancy of 0.5. The density for the −1 MurNAc residue is not very clear. Several different orientations may be present for this residue. In the model presented here, the −1 MurNAc has been modeled in the energetically most favorable $^4C_1$ chair conformation, with the O1 hydroxyl group in a β-anomeric configuration.

The GlcNAc residue at subsite −2 has a full $^4C_1$ chair conformation and binds with its *N*-acetyl group in a cavity that predominantly consists of the aromatic rings of Phe226, Tyr259, and Tyr338. The *N*-acetyl group is within hydrogen bonding distance of the Ser230 Oγ atom and the Met227 N atom. The O3-hydroxyl group may form a hydrogen bond to the Tyr259 side chain, whereas the O6-hydroxyl group is within hydrogen bonding distance of the carbonyl oxygen atom of the L-Ala residue at subsite −1.

The MurNAc-L-Ala-D-Glu moiety of murodipeptide A binds in subsite −1. The electron density for the *N*-acetyl group permits two orientations with the group pointing either upward or downward. In the down position, it has no interactions with protein or ligand atoms, while in the up position, its O7 and N2 atoms are within hydrogen bonding distance of Gln98 and a water molecule bound to Ser216, respectively. The position of the MurNAc O1 atom is uncertain, because of its lack of electron density. The O6-hydroxyl group is within hydrogen bonding distance of Tyr338 and Glu162 (Figure 4A). The D-lactyl moiety and

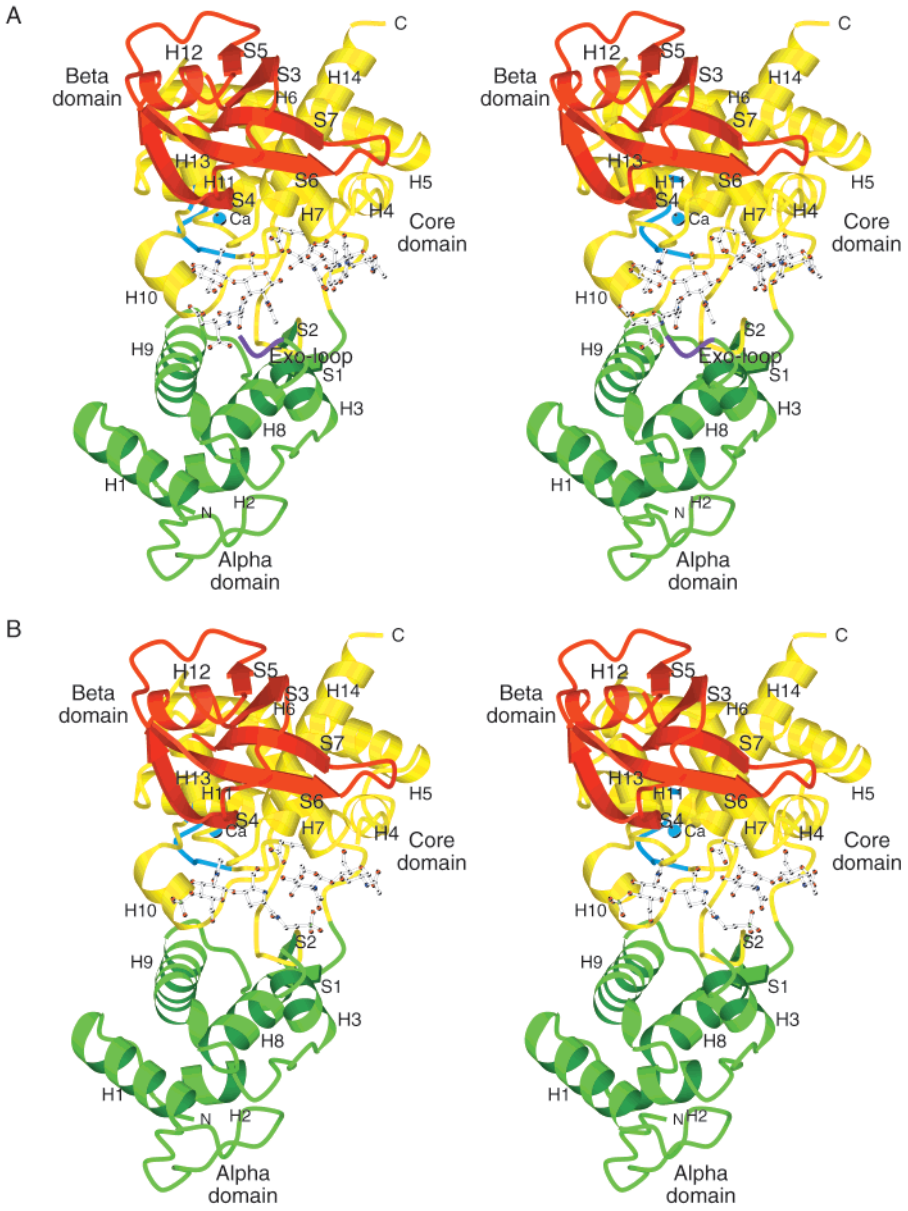

FIGURE 2: Stereoviews of Slt35−substrate complexes with domain and secondary structure labeling. (A) The Slt35−murodipeptide complex with murodipeptide A in subsites −2 and −1 and murodipeptide B in subsites +1 and +2. (B) The Slt35−bulgecin A−chitobiose complex with bulgecin A in subsites −2 and −1 and chitobiose in subsites +1 and +2. The catalytic acid/base Glu162 is located between subsites −1 and +1. Glu162, the substrates, and the calcium ion in the EF-hand calcium-binding site are shown as ball-and-stick representations. The α, *β*, and core domains are colored green, red, and yellow, respectively, while the EF-hand loop (residues 237−245) and the calcium ion are colored light blue. The residues of the exo-loop (residues 99−108) run from α-helix H3 to α-helix H4, but due to flexibility, most of these residues could not be identified in the electron density maps. Only for the Slt35−murodipeptide and Slt35−bulgecin A complexes electron density was present for residues 99 and 100 of the exo-loop (magenta in panel A), and therefore, these residues could be included in the models. This figure was produced with MOLSCRIPT (*36*).

the dipeptide are stabilized by Arg188 and Arg187, respectively. Interestingly, the bound murodipeptide A seems to stabilize residues 99 and 100 of the exo-loop (residues 99−108), which were not visible in the native 1.7 Å Slt35 structure. This is probably due to hydrophobic interactions between Pro100 and the dipeptide moiety of murodipeptide A.

Murodipeptide B binds with its GlcNAc residue in subsite +1, and the MurNAc-L-Ala-D-Glu moiety at subsite +2. Both GlcNAc and MurNAc exhibit clear density for a $^4C_1$ chair conformation (Figure 3A). GlcNAc is within hydrogen bonding distance of Glu162 and Asn339, while the +2 MurNAc-L-Ala-D-Glu moiety might form hydrogen bonds with residue 161 and His343 (Figure 4A). The MurNAc residue clearly exhibits electron density for an O1-hydroxyl group in an α-anomeric configuration, which is probably due to the formation of a hydrogen bond between the O1 atom and the side chain of Gln207 of a symmetry-related molecule. The L-Ala-D-Glu dipeptide makes mainly van der Waals and hydrophobic interactions with the side chains of Tyr117, Lys120, and Phe121.

Slt35−Bulgecin A Complex. Bulgecin A is bound in an extended conformation with the GlcNAc residue in a $^4C_1$ chair conformation at the −2 subsite and the hydroxyproline residue at the −1 subsite (Figure 4B). The GlcNAc residue occupies the same position as the GlcNAc residue of

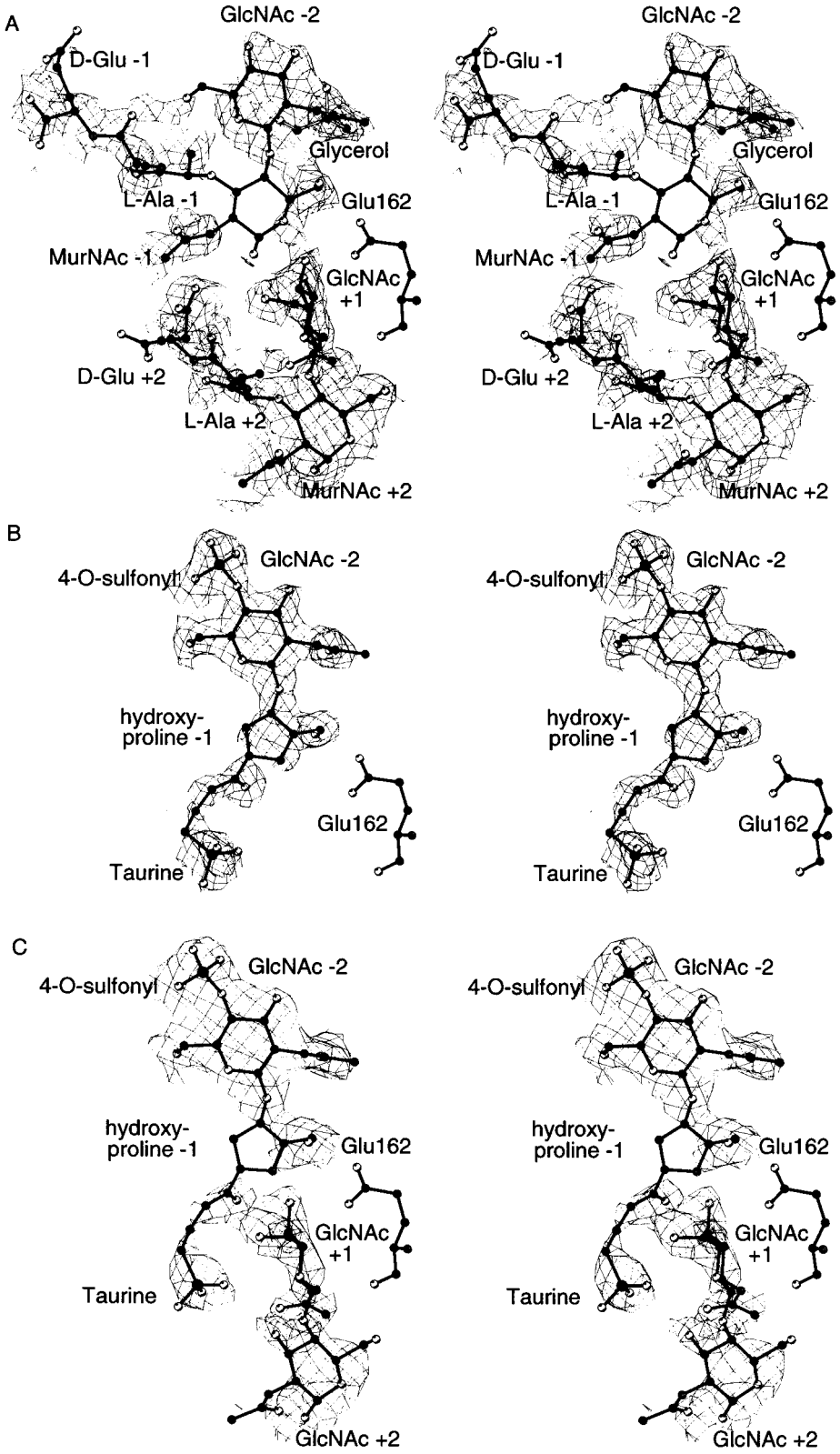

FIGURE 3: Stereoviews of the Slt35 complexes superimposed on the simulated annealing omit and σ_A-weighted $F_o - F_c$ electron density maps. (A) Murodipeptides A and B (black bonds) and glycerol (white bonds) in the Slt35−murodipeptide complex. (B) Bulgecin A in the Slt35−bulgecin A complex. (C) Bulgecin A and chitobiose in the Slt35−bulgecin A−chitobiose complex. The superimposed electron density maps are contoured at the 2.0σ level for the Slt35−bulgecin A and Slt35−bulgecin A−chitobiose complexes and at the 1.5σ level for the Slt35−murodipeptide complex. The densities have been calculated from the final models excluding the particular molecule(s) using a standard simulated annealing protocol in X-PLOR (*37*, *38*). The substrate atoms and Glu162 are shown as ball-and-stick representations with carbon atoms in black, nitrogen atoms in gray, oxygens in white, and sulfur atoms as larger gray balls.

murodipeptide A (see above) and forms the same hydrogen bonds. However, due to small protein movements (see below), the O6-hydroxyl group is now within hydrogen bonding distance of the side chains of Arg188 and Tyr191. Furthermore, the *N*-acetyl nitrogen is now within hydrogen bonding distance of the carbonyl oxygen of Tyr338 (Figure

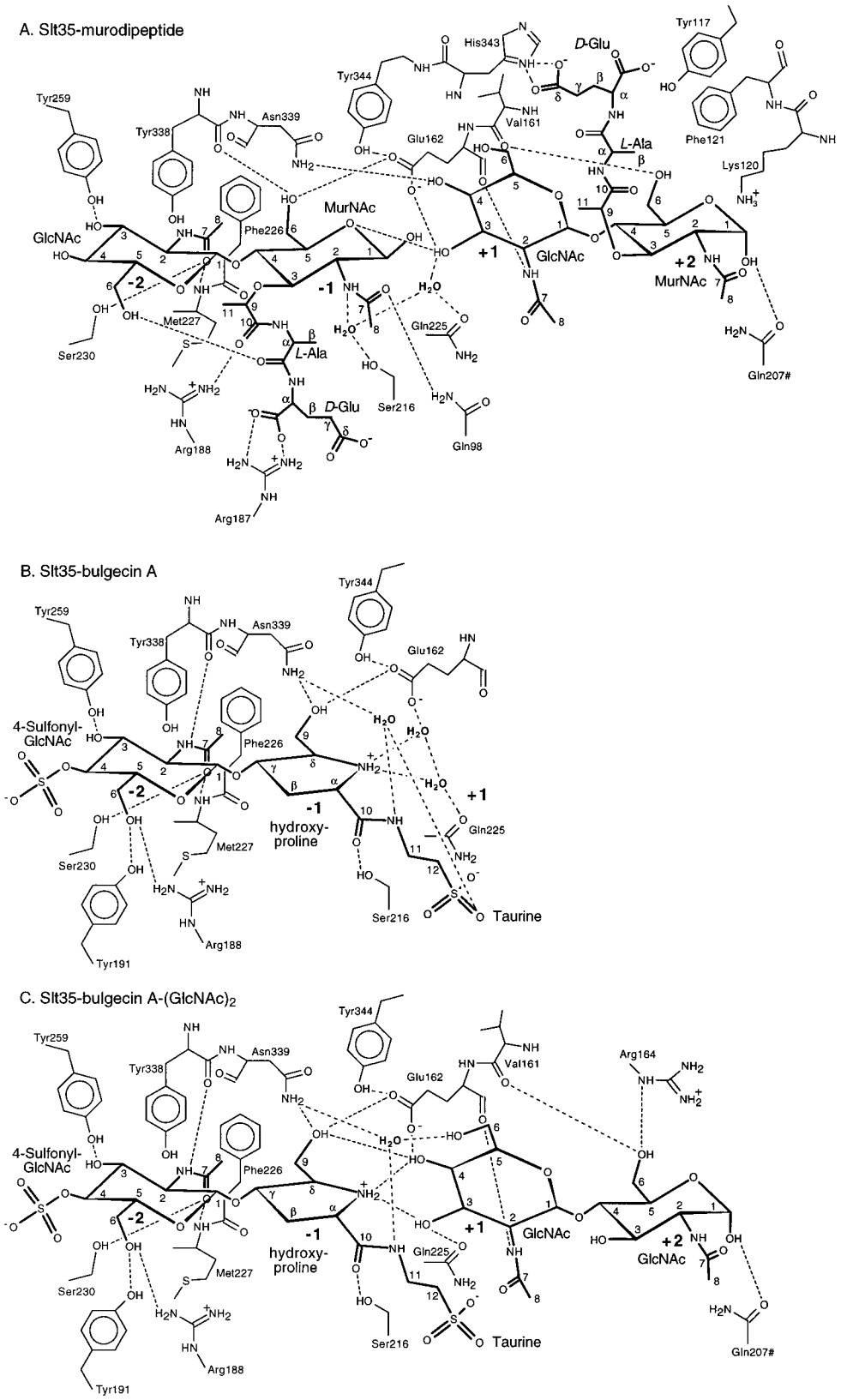

FIGURE 4: Schematic drawing of the hydrogen bonding interactions (dotted lines) in the Slt35 complexes. (A) The Slt35−murodipeptide complex. (B) The Slt35−bulgecin A complex. (C) The Slt35−bulgecin A−chitobiose complex. In all three structures, Glu162 is displayed as a base, although the acid form cannot be excluded. Residue Gln207# is from a symmetry-related molecule.

4B). The GlcNAc 4-*O*-sulfonate group has no direct hydrogen bonding interactions with the protein.

At subsite −1, the 5-hydroxymethyl oxygen of the modified hydroxyproline residue is within hydrogen bonding distance of the Oϵ2 atom of Glu162 and the Nδ2 atom of Asn339, respectively. The carbonyl oxygen of the hydroxyproline moiety may form a hydrogen bond to the Oγ of Ser216. Probably, a weak electrostatic interaction is present between the carboxylate group of Glu162 and the amine nitrogen in the proline ring (distance of 4.1 Å). This atom is

most likely protonated at the pH of the experiment (pH 8.0), as the pK_a of this group is about 10.6 (*25*).

The taurine residue ($NHCH_2CH_2SO_3$) is linked to the carbonyl group of the hydroxyproline via a peptide bond. The sulfonyl group has no direct hydrogen bonds with Slt35. Its atomic displacement parameters are higher than those of the rest of bulgecin (between 50 and 60 Å^2), suggesting flexibility. The N10 atom of the taurine residue may form two water-mediated hydrogen bonds: one to the Nδ2 atom of Asn339 and one to a sulfonyl oxygen of the taurine.

Bulgecin A is an effective inhibitor of the lytic transglycosylase Slt70 of *E. coli* (*6*), but less so of Slt35 (*16*). In an attempt to understand this difference, we compared the binding modes of bulgecin A in Slt70 (*26*) and Slt35. In both enzymes, the inhibitor binds in a similar extended conformation. However, in Slt70 the N10 atom of bulgecin A makes a hydrogen bond to the carboxylate group of Glu583, but to a water molecule in Slt35. Both the Glu583 side chain and the water molecule are within hydrogen bonding distance of the Nδ2 atom of a conserved asparagine residue (Asn553 in Slt70 and Asn339 in Slt35). Second, the O3 atom of the GlcNAc residue in bulgecin A makes two hydrogen bonds in Slt70 (to the Oη atom of Tyr533 and the Oγ1 atom of Thr501), but one in Slt35 (to the Oη atom of Tyr259). Third, the O6 atom of bulgecin A cannot form hydrogen bonds in Slt70, but in Slt35, it is within hydrogen bonding distance of the Nη2 of Arg188 and the Oη of Tyr191, residues without an equivalent in Slt70. Fourth, bulgecin A has extra van der Waals interactions with Slt70 residues Ala554, Gly555, and Pro556 (forming a loop above subsites −2 and −1). These residues are absent in Slt35. Finally, bulgecin A has a tighter fit in the active site of Slt70. The volume of the bulgecin binding pocket is 635 Å^3 in Slt70 and 719 Å^3 in Slt35, as calculated with the program GRASP (*27*). Taken together, these differences may explain why bulgecin A is a better inhibitor of Slt70 than of Slt35.

Slt35−Bulgecin A−Chitobiose Complex. In the ternary complex of Slt35 with bulgecin A and chitobiose, the bulgecin molecule is bound at subsites −2 and −1 in a fashion similar to that found in the Slt35−bulgecin A complex (Figures 2B, 3C, and 4C). Chitobiose is bound at subsites +1 and +2, but in a manner different from that of the sugar residues of murodipeptide B (Figure 5). On average, the ring atoms of the +1 and +2 sugars are displaced by 1.6 and 0.6 Å, respectively. The O6-hydroxyl group of the +2 GlcNAc of chitobiose may form hydrogen bonds to the carbonyl oxygen atom of Val161 and the Nϵ atom of Arg164. The latter hydrogen bond cannot be formed in the Slt35−murodipeptide B complex, because of a different rotamer conformation of the arginine side chain. Like murodipeptide B, the +2 sugar has its O1 atom in an α-anomeric configuration stabilized by the side chain of Gln207 of a symmetry-related molecule.

Whereas the Oϵ1 atom of Glu162 is hydrogen bonded to the O3-hydroxyl group of the +1 GlcNAc residue in the Slt35−murodipeptide complex, in the Slt35−bulgecin A−chitobiose complex it is within hydrogen bonding distance of the O4-hydroxyl group of the +1 GlcNAc. Since the Oϵ1 atom of Glu162 is supposed to donate a proton to the O4 of the +1 GlcNAc, it seems likely that the binding of chitobiose resembles more the sugar binding of peptidoglycan to Slt35 than the binding of the murodipeptide B.

Comparison with Peptidoglycan Binding in Slt70. The catalytic domains of Slt35 and Slt70 are very similar [root-mean-square deviation of 1.7 Å for 100 Cα atoms (*9*)]. A comparison of the observed +1 GlcNAc binding modes in Slt35 and Slt70 shows that the +1 GlcNAc residue of the Slt35−bulgecin A−chitobiose complex is in a position similar to the +1 GlcNAc in the Slt70−1,6-anhydro-muropeptide complex (ref *28* and Figure 5B). The +1 GlcNAc residues have conserved hydrogen bonding interactions in both proteins with their O3 atoms (to the Oϵ1 atom of the conserved Gln225 and Gln496 in Slt35 and Slt70, respectively), their O4 atoms (to the Oϵ1 atom of the catalytic acid/base Glu162 and Glu478 in Slt35 and Slt70, respectively), and their N2 atoms (to the backbone carbonyl oxygen of the catalytic acid/base). In contrast, the +1 GlcNAc residue of the Slt35−murodipeptide complex occupies a different position and makes only the latter conserved hydrogen bond. Because a tight binding of the +1 GlcNAc residue is important to preventing hydrolysis of the reaction intermediate (see Discussion), this strengthens the above conclusion that the chitobiose molecule in the Slt35−bulgecin A−chitobiose complex resembles more a competent peptidoglycan binding mode in subsites +1 and +2 than the murodipeptide B.

An intriguing difference between Slt35 and Slt70 is the hydrophobicity of their +1 sites. Val161 in Slt35 is substituted for a glutamine residue in Slt70 (Gln477). The shorter and hydrophobic valine side chain in Slt35 creates a hydrophobic pocket, which can accommodate the C6 atom of the +1 GlcNAc with favorable van der Waals and hydrophobic interactions with the side chains of Val161, Phe121, and Tyr344. In Slt70, a hydrogen bonding interaction is present between the Oϵ1 atom of Glu477 and the O6 atom of the +1 GlcNAc.

Active Site Plasticity. The structural differences between native Slt35 (*9*), the Slt35−GlcNAc complex (*9*), and the three Slt35 structures presented here were studied by superimposing their backbone N, Cα, and C atoms. The most significant difference is observed in the active site after binding of bulgecin A and the GlcNAc molecule in subsite −2 (Figure 5A), which induces a displacement of the main chain atoms of Tyr338, Asn339, and His340 by up to 0.9 Å in the various complex structures with respect to the native structure. This displacement is accompanied by the formation of a hydrogen bond between the carbonyl oxygen atom of Tyr338 and the N2 of the −2 GlcNAc residue in the Slt35−GlcNAc and Slt35−bulgecin A complexes. This hydrogen bond is not observed in the Slt35−murodipeptide complex, which might be due to the partial occupancy. Furthermore, the displacement allows a hydrogen bond to be formed between the Nδ2 atom of Asn339 and the O9 atom of bulgecin A, which is in a position similar to the O6 atom of the −1 MurNAc.

A second significant difference concerns residues Arg187 and Arg188 in the Slt35−bulgecin A complexes, of which the main chain atoms have moved about 0.7−1.0 Å further into the active site compared to those in the native structure. Both residues are involved in substrate binding. Their movement results in a further narrowing of the active site cleft and might optimize the hydrogen bonding interactions with the peptide side chain of the −1 MurNAc.

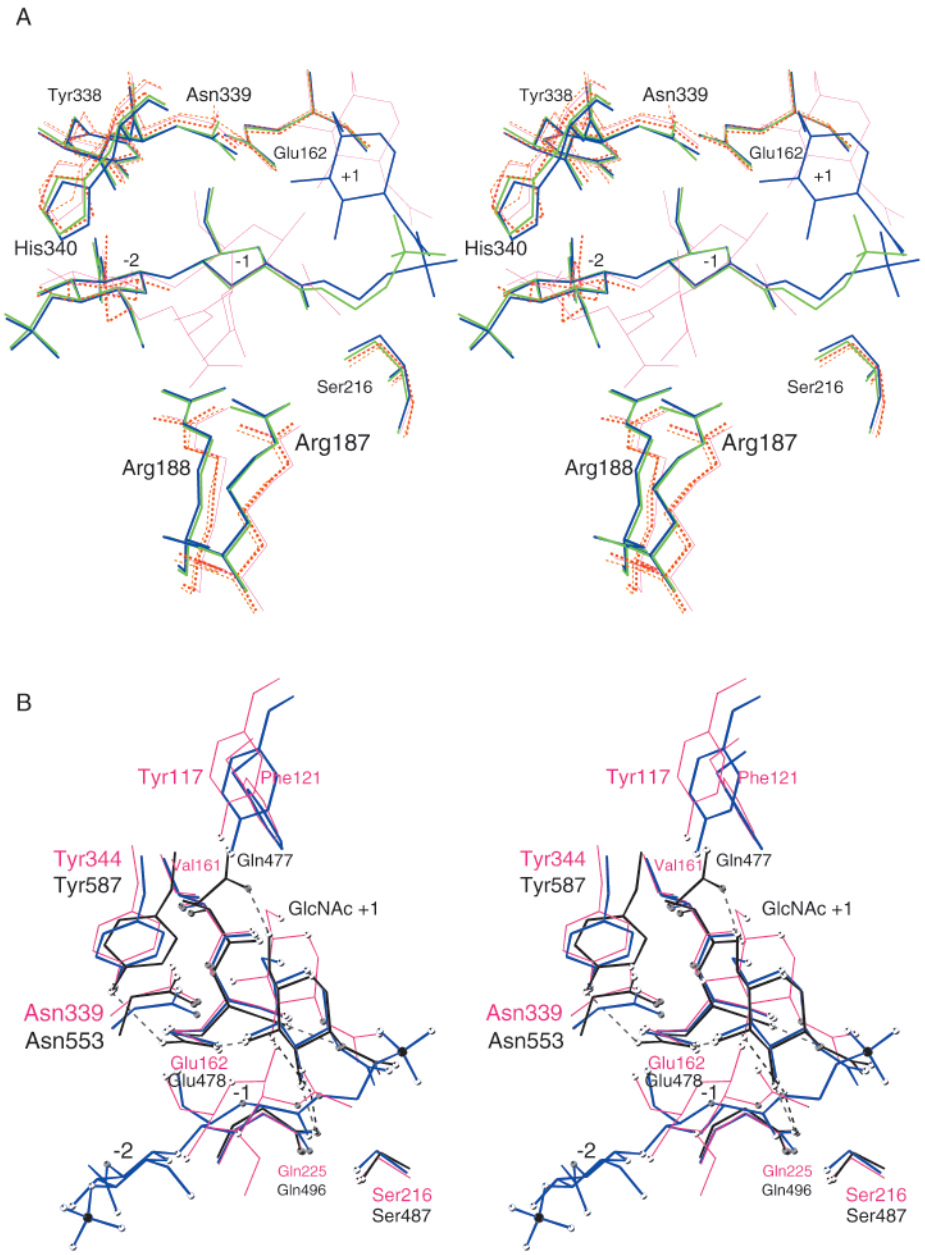

FIGURE 5: Stereoviews of superpositions of Slt35 and Slt70 made with O (*22*) and DYNDOM (*39*). (A) Superpositions of the active sites of the Slt35 complexes using residues of the core domain (123−136, 148−162, 164−169, 220−261, and 351−359). Thin orange dashed lines represent native Slt35, thick red dashed lines Slt35−GlcNAc, thin pink lines Slt35−murodipeptide, thick green lines Slt35−bulgecin A, and thick blue lines Slt35−bulgecin A−chitobiose. (B) Superposition of the +1 subsite of the Slt35−murodipeptide B complex (pink bonds), the Slt35−bulgecin A−chitobiose complex (blue bonds), and the Slt70−1,6-anhydromuropeptide complex (black bonds). The Slt35 complexes were superimposed on each other as described for panel A. The Slt70−1,6-anhydromuropeptide complex was superimposed on the Slt35 complexes using the LSQ option in the program O (*22*) by aligning Gln477, Glu478, Ser487, Gln496, and Tyr552 of Slt70 on Val161, Glu162, Ser216, Gln225, and Tyr338 of Slt35, respectively. For clarity, only the GlcNAc residue of the 1,6-anhydromuropeptide in Slt70 is shown. The black labels refer to Slt70 residues, while the pink labels refer to Slt35 residues.

DISCUSSION

Peptidoglycan-Binding Cleft. This study shows that the *E. coli* lytic transglycosylase Slt35 contains at least four sugar-binding sites. GlcNAc residues bind in subsites −2 and +1 and MurNAc residues in subsites −1 and +2. Near the MurNAc binding sites are two peptide-binding regions. So far, only two other crystal structures of a protein complexed with a muropeptide have been elucidated: the T26E mutant of phage T4 lysozyme (T4L) complexed with the murotetrapeptide (GlcNAc-MurNAc-L-Ala-D-Glu-*m*-Dap-D-Ala) in subsites −2 and −1 (*29*) and Slt70 complexed with a 1,6-anhydromurotripeptide (GlcNAc-anhMurNAc-L-Ala-D-Glu-*m*-Dap) in subsites +1 and +2 (*28*). The catalytic domains of Slt35, Slt70, and T4L have a similar fold with a comparable substrate-binding groove. Comparison of the complexes shows that both Slt35 and T4L bind a GlcNAc residue in subsite −2 with the GlcNAc residues making similar interactions with an aromatic residue (Tyr338 in Slt35 and Phe104 in T4L) and a hydrophobic residue (Met227 in Slt35 and Leu32 in T4L). Furthermore, these two proteins bind a MurNAc residue in subsite −1. In both enzymes, the MurNAc O6 atom is within hydrogen bonding distance of the Oϵ2 atom of the catalytic glutamic acid (Glu162 in Slt35 and Glu11 in T4L), and the free Cα carboxylate group of

the D-Glu residue in the MurNAc peptide side chain makes a salt bridge to an arginine residue (Arg187 in Slt35 and Arg137 in T4L). Notwithstanding these similarities, it should be noted that in the T4L mutant the −1 MurNAc residue is covalently bound (to Glu26), but not in Slt35. In Slt35, Ala220 is in a position equivalent to that of Glu26 in the T4L mutant and its Cβ atom has a hydrophobic interaction with the C5 atom of the −1 MurNAc residue.

Comparison of the Slt35−bulgecin A−chitobiose complex and the Slt70−1,6-anhydromurotripeptide complex shows that in both enzymes the O4 atom of the +1 GlcNAc is hydrogen bonded to the Oϵ1 atom of the catalytic acid/base (Glu162 in Slt35 and Glu478 in Slt70). This hydrogen bond may mimic the interaction of the catalytic Glu with the glycosidic oxygen of the scissile bond during the cleavage reaction.

Reaction Mechanism. Lytic transglycosylases catalyze the cleavage of the β-1,4-glycosidic bond between MurNAc and GlcNAc with concomitant formation of a 1,6-anhydro bond in the MurNAc residue. They use a Glu as an acid/base to facilitate the reaction. In Slt35, Glu162 is located between the −1 and +1 subsites in a hydrophobic environment created by the side chains of Ile158, Gln225, Tyr338, and Tyr344. This environment stabilizes the protonated state of Glu162 at the optimum pH of the reaction (pH 5.0), which enables Glu162 to have a hydrogen bonding interaction with the glycosidic oxygen of the scissile bond. It is the only acid in the peptidoglycan-binding cleft of Slt35, and its position coincides with the catalytic acid/base Glu478 of Slt70 after superposition (*9*). Furthermore, a Glu162Gln mutation yielded an inactive enzyme (*9*). From this, we conclude that Glu162 is the catalytic acid/base in the reaction catalyzed by Slt35.

During the cleavage reaction, a positively charged oxocarbonium ion-like intermediate is likely to occur. The oxocarbonium ion should be shielded from the solvent to allow attack by the −1 MurNAc O6 atom and to prevent a hydrolysis reaction. For Slt70, it has been proposed that the NH_2^+ moiety of the bulgecin hydroxyproline mimics the oxocarbonium ion intermediate (*26*). If this is also true for Slt35, the bulgecin NH_2^+ group should be shielded from the solvent as well. Comparison of the binary and ternary Slt35−bulgecin A complexes shows that the +1 GlcNAc O3 and O4 atoms replace two water molecules that interact with the −1 hydroxyproline NH_2^+ group of bulgecin (Figure 4B,C). These water molecules could mimic the hydrolytic water molecule attacking the oxocarbonium intermediate. Thus, a prolonged presence of a GlcNAc residue in the +1 site could prevent such a hydrolysis reaction.

The peptide bond between the hydroxyproline and taurine parts of bulgecin A is supposed to mimic an *N*-acetyl group that stabilizes the oxocarbonium ion intermediate (*26*). In Slt70, the O and N atoms of this peptide bond are hydrogen bonded to the Oγ of Ser487 and the carboxylate group of Glu583, respectively. In Slt35, Ser216 occupies a position equivalent to Ser487 and forms a hydrogen bond to the taurine peptide carbonyl oxygen atom. No residue has been identified in Slt35 that can take over the role of Glu583 of Slt70. Nevertheless, a superposition of the substrate complexes of Slt35 and Slt70 shows that around the position of the Glu583 carboxylate group in Slt70, five hydrogen bond donors are present in Slt35: Nδ2 of Asn339, Nϵ2 of Gln98, NH of L-Ala in subsite −1, N10 of bulgecin A (which would correspond to the N2 of a MurNAc residue), and the O6-hydroxyl group of GlcNAc in subsite +1. Because a free carboxylate group can accept four to five hydrogen bonds, it is tempting to assume that these hydrogen bond donors create a binding site for a free carboxylate group, which can stabilize the reaction intermediate. Such a carboxylate group could come from the peptidoglycan substrate itself, which would explain why the peptide chains of peptidoglycan are absolutely required for activity (*16*). One possibility would be the free carboxylate group of the −1 D-Glu residue. This group makes, however, a salt bridge to the side chain of Arg187 and is therefore unlikely to supply the stabilizing carboxylate group. However, the +2 D-Glu residue has a free carboxylate group which can be modeled into the carboxylate binding pocket (data not shown).

On the basis of our crystallographic studies and what is known for Slt70 (*26*) and other polysaccharide-degrading enzymes (*30*, *31*), we propose the following reaction mechanism for Slt35 (Figure 6). In the first step, Slt35 binds the nonreducing end of a peptidoglycan strand at subsites −2, −1, +1, and +2 (see Table 2 for the Slt35 residues involved in the binding of peptidoglycan). The terminal GlcNAc residue is bound in subsite −2, because Slt35 acts as an exo-muramidase, which starts at the nonreducing GlcNAc end of a peptidoglycan strand and processively releases 1,6-anhydromuropeptides (*9*, *16*). Binding of peptidoglycan at subsites −2 and −1 triggers small active site movements (induced fit), which allow optimization of the binding interactions. The *N*-acetyl group of the −1 MurNAc is oriented and stabilized by Ser216. The free carboxylate of the −2 D-Glu may interact with the *N*-acetyl group as well. The MurNAc sugar ring is believed to be distorted from a ground-state chair into the more reactive sofa conformation. A distortion of the −1 sugar from the ground state to the sofa form would optimize the overlap of the C1−O4 σ^* antibonding orbital and one of the lone pairs of the O5 atom and thereby weaken the C1−O4 bond (*32*). The weakened scissile bond can now easily be cleaved with concomitant protonation of the glycosidic O4 oxygen by the protonated Oϵ1 atom of Glu162. Cleavage of the glycosidic bond results in the formation of a positively charged −1 MurNAc oxocarbonium ion and a negatively charged Glu162. The negative charge of the Glu162 carboxylate group may be stabilized by three hydrogen bonds with the Tyr344 hydroxyl group, the −1 MurNAc O6-hydroxyl group, and the +1 GlcNAc O4-hydroxyl group. The positively charged oxocarbonium ion is probably stabilized by the *N*-acetyl oxygen of MurNAc, either by a charge−charge interaction or by a covalent oxazolinium intermediate. This is similar to what has been proposed for Slt70 (*26*) and chitin-degrading enzymes (*30*, *33*). The reaction intermediate in Slt35 is shielded from the solvent by the *N*-acetyl group of the −1 MurNAc, the +1 GlcNAc, the +2 D-Glu, and Asn339, which prevents a nucleophilic attack by a water molecule. To form the 1,6-anhydro bond, the MurNAc residue needs to change from a sofa into a boat conformation to bring the O6 atom closer to the C1 atom for nucleophilic attack. Thereby, the Oϵ2 atom of Glu162 could enhance the nucleophilicity of the O6 atom by abstracting its proton. This would result in the formation of a negatively charged O6 atom, which might be stabilized by Asn339. In the Slt35−bulgecin A complexes,

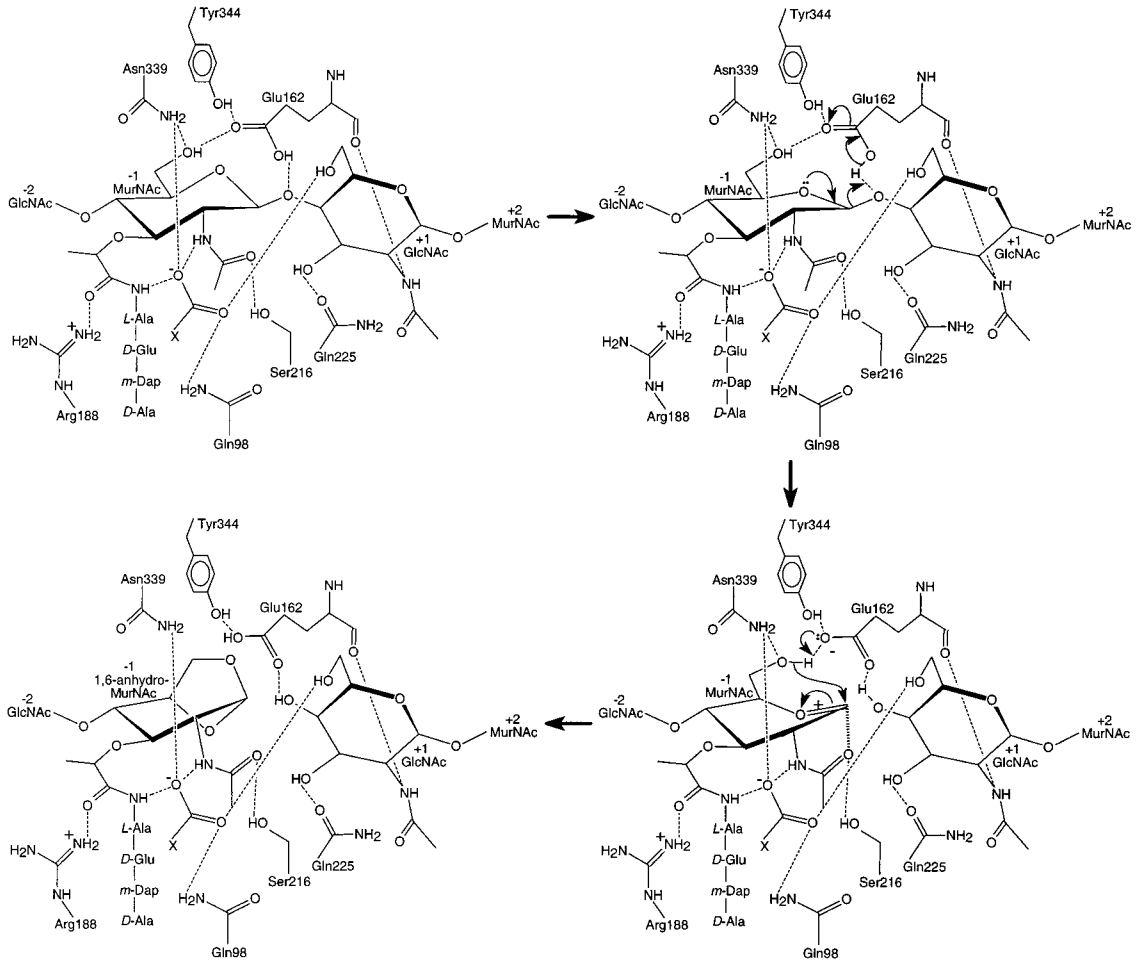

FIGURE 6: Proposed reaction mechanism of Slt35 (see the text for an explanation). The X indicates a carboxylate group of peptidoglycan.

Table 2: Residues in the Peptidoglycan-Binding Cleft of Slt35[a]

subsite −2	GlcNAc	Arg188, Tyr191, Gly224, Gln225, Phe226, Met227, Ser230, Tyr259, Arg337, Tyr338, His340
subsite −1	MurNAc	Met95, Gln98, Glu162, Arg188, Tyr191, Phe192, Ser216, Ala218, Ala220, Gln225, Met227, Tyr338, Asn339, Tyr344
	L-Ala	Gln98, Arg188
	D-Glu	Gln98, Ala99, Pro100, Arg187, Arg188, His340
subsite +1	GlcNAc	Tyr117, Phe121, Val161, Glu162, Val168, Met169, Gln170, Ser216, Gln225, Asn339, Tyr344
subsite +2	MurNAc	Lys120, Phe121, Gly160, Val161, Glu162, Thr163, Arg164, Val168
	L-Ala	Tyr117, Lys120, Phe121
	D-Glu	Tyr117, His343

[a] Residues of Slt35 within 4.5 Å of murodipeptides A and B, bulgecin A, and $(GlcNAc)_2$. The underlined residues are or can be involved in the hydrogen bonding with the peptidoglycan residues (within 3.5 Å) based on the three crystal structures.

the Nδ2 atom of Asn339 is found within hydrogen bonding distance of the O9 atom of bulgecin A, which is in a position similar to the −1 MurNAc O6 atom. It is therefore probable that Asn339 facilitates the proton abstraction of the O6 atom by Glu162. The subsequent attack by the O6 atom on the positively charged C1 atom would yield the 1,6-anhydro bond in the MurNAc residue. Finally, the 1,6-anhydro-muropeptide is released, and the GlcNAc and MurNAc residues in subsites +1 and +2 may move to subsites −2 and −1. The enzyme is now ready for a new catalytic cycle.

The study presented here shows that three residues in subsite −1 of Slt35 may play an important role in the binding and cleavage of peptidoglycan: Glu162, Ser216, and Asn339. In *E. coli* Slt70, the equivalent residues are Glu478, Ser487, and Asn553. These three residues are strictly conserved among all known MltB/Slt35 and Slt70 lytic transglycosylases, as shown by amino acid sequence analyses (*9*, *28*). Site-directed mutagenesis studies have already shown that mutation of the catalytic Glu into a Gln residue resulted in inactive enzymes (*7*, *9*). Mutation of the other two residues could unambiguously demonstrate their importance in the reaction mechanism of lytic transglycosylases.

ACKNOWLEDGMENT

We thank Dr. A.-M. W. H. Thunnissen for critical reading of the manuscript and Dr. A. J. Dijkstra and Dr. W. Keck (F. Hoffmann-LaRoche Ltd.) for stimulating discussions and the supply of bulgecin A. We are grateful to the staff of DESY for their help during data collection and to the European Union for support of the work at the EMBL Hamburg through the TMR/LSF programme (Contract ERBFMGECT980134).

REFERENCES

1. Höltje, J.-V., Mirelman, D., Sharon, N., and Schwarz, U. (1975) *J. Bacteriol. 124*, 1067−1076.
2. Höltje, J.-V. (1995) *Arch. Microbiol. 164*, 243−254.
3. Höltje, J.-V., and Tuomanen, E. I. (1991) *J. Gen. Microbiol. 137*, 441−454.
4. Goodell, E. W. (1985) *J. Bacteriol. 163*, 305−310.
5. Dijkstra, A. J., and Keck, W. (1996) *J. Bacteriol. 178*, 5555−5562.
6. Templin, M. F., Edwards, D. H., and Höltje, J.-V. (1992) *J. Biol. Chem. 267*, 20039−20043.
7. Thunnissen, A.-M. W. H., Dijkstra, A. J., Kalk, K. H., Rozeboom, H. J., Engel, H., Keck, W., and Dijkstra, B. W. (1994) *Nature 367*, 750−753.
8. van Asselt, E. J., Perrakis, A., Kalk, K. H., Lamzin, V. S., and Dijkstra, B. W. (1998) *Acta Crystallogr. D 54*, 58−73.
9. van Asselt, E. J., Dijkstra, A. J., Kalk, K. H., Takacs, B., Keck, W., and Dijkstra, B. W. (1999) *Structure 7*, 1167−1180.
10. Engel, H., Smink, A. J., van Wijngaarden, L., and Keck, W. (1992) *J. Bacteriol. 174*, 6394−6403.
11. Dijkstra, A. J., Hermann, F., and Keck, W. (1995) *FEBS Lett. 366*, 115−118.
12. Ehlert, K., Höltje, J.-V., and Templin, M. F. (1995) *Mol. Microbiol. 16*, 761−768.
13. Davies, G. J., Wilson, K. S., and Henrissat, B. (1997) *Biochem. J. 321*, 557−559.
14. van Asselt, E. J., and Dijkstra, B. W. (1999) *FEBS Lett. 458*, 429−435.
15. Beachey, E. H., Keck, W., de-Pedro, M. A., and Schwarz, U. (1981) *Eur. J. Biochem. 116*, 355−358.
16. Romeis, T., Vollmer, W., and Höltje, J.-V. (1993) *FEMS Microbiol. Lett. 111*, 141−146.
17. Shinagawa, S., Kasahara, F., Wada, Y., Harada, S., and Asai, M. (1984) *Tetrahedron 40*, 3465−3470.
18. Nakao, M., Yukishige, K., Kondo, M., and Imada, A. (1986) *Antimicrob. Agents Chemother. 30*, 414−417.
19. Otwinowski, Z., and Minor, W. (1997) *Methods Enzymol. 276*, 307−326.
20. Brünger, A. T. (1992) *Nature 355*, 472−475.
21. Brünger, A. T. (1992) *X-PLOR. A system for crystallography and NMR*, Yale University Press, New Heaven, CT.
22. Jones, T. A., Zou, J.-Y., Cowan, S. W., and Kjeldgaard, M. (1991) *Acta Crystallogr. A 47*, 110−119.
23. Weis, W. I., Brünger, A. T., Skehel, J. J., and Wiley, D. C. (1990) *J. Mol. Biol. 212*, 737−761.
24. Laskowski, R. A., MacArthur, M. W., Moss, D. S., and Thornton, J. M. (1993) *J. Appl. Crystallogr. 26*, 283−291.
25. Weast, R. C. (1982) *Handbook of Chemistry and Physics*, 63rd ed., CRC Press, Boca Raton, FL.
26. Thunnissen, A.-M. W. H., Rozeboom, H. J., Kalk, K. H., and Dijkstra, B. W. (1995) *Biochemistry 34*, 12729−12737.
27. Nicholis, A., Sharp, K. A., and Honig, B. (1991) *Proteins: Struct., Funct., Genet. 11*, 281−296.
28. van Asselt, E. J., Thunnissen, A.-M. W. H., and Dijkstra, B. W. (1999) *J. Mol. Biol. 291*, 877−898.
29. Kuroki, R., Weaver, L. H., and Matthews, B. W. (1993) *Science 262*, 2030−2033.
30. Tews, I., Terwisscha van Scheltinga, A. C., Perrakis, A., Wilson, K. S., and Dijkstra, B. W. (1997) *J. Am. Chem. Soc. 119*, 7954−7959.
31. White, A., and Rose, D. R. (1997) *Curr. Opin. Struct. Biol. 7*, 645−651.
32. Sinnot, M. L. (1990) *Chem. Rev. 90*, 1171−1202.
33. Terwisscha van Scheltinga, A. C., Armand, S., Kalk, K. H., Isogai, A., Henrissat, B., and Dijkstra, B. W. (1995) *Biochemistry 34*, 15619−15623.
34. Engh, R. A., and Huber, R. (1991) *Acta Crystallogr. A 47*, 392−400.
35. Shinagawa, S., Maki, M., Kintaka, K., Imada, A., and Asai, M. (1985) *J. Antibiot. 38*, 17−23.
36. Kraulis, P. J. (1991) *J. Appl. Crystallogr. 24*, 946−950.
37. Hodel, A., Kim, S.-H., and Brünger, A. T. (1992) *Acta Crystallogr. A 48*, 851−859.
38. Read, R. J. (1986) *Acta Crystallogr. A 42*, 140−149.
39. Hayward, S., and Berendsen, H. J. C. (1998) *Proteins 30*, 144−154.

BI992161P